

Detection of Cloud-Top Height from Backscattered Radiances within the Oxygen A Band. Part 1: Theoretical Study

J. FISCHER

GKSS-Forschungszentrum, Geesthacht, Germany

H. GRASSL

Max-Planck-Institut für Meteorologie, Hamburg, Germany

(Manuscript received 10 January 1990, in final form 20 January 1991)

ABSTRACT

A series of radiative transfer calculations were performed to study the possibility of determining cloud-top pressure (height) from backscattered solar radiances within the oxygen A-band absorption. For the development of a cloud-top pressure algorithm, we also looked into the impact of perturbing effects, such as varying cloud properties, sun elevation, and surface albedo. The most important quantities are total cloud optical thickness δ_C and the vertical profile of liquid-water content.

The effects of cloud optical thickness—if $\delta_C > 1$ —are already taken into account by a cloud-top algorithm, which only considers two radiances inside and outside the oxygen absorption band. For one-layer clouds, the cloud-top heights may be derived to within an accuracy of 200 m. Multilayer clouds or varying liquid-water content profiles can only be matched with an inverse technique using radiances at up to 16 wavelengths, which, however, give cloud-top height estimates to within an error of only 50 m for all 900 cloud cases considered.

1. Introduction

The radiation balance of the earth-atmosphere system is significantly altered by clouds. Over 50% of the earth is covered by clouds. They determine the amount of solar radiation scattered back into space and block the terrestrial radiation from the earth's surface into space. More precise climate studies will be possible only if cloud properties are more realistically incorporated into numerical global circulation models. In order to assess the clouds' impact on the radiation budget, many cloud properties are required: cloud-top height (pressure), optical thickness, cloud-droplet-size distribution, cloud temperature, and cloud-size distribution. The importance of a cloud-top pressure detector has already been emphasized by Ohring and Adler (1978), who found that an increase of 1 km in cloud height would result in a 1.2 K increase in surface temperature. However, a concomitant increase in cloud-base height would reduce the increase to only 0.6 K, thus, damping the additional greenhouse effect by higher clouds.

For the estimation of cloud properties from satellite data, several methods have been proposed in recent years: stereoscopic imagery for cloud heights (Shenk

et al. 1975), a bispectral method for inferring both cloud amount and cloud-top temperature from observations in the visible and 11 μm (Vonder Haar and Reynolds 1974), cloud-height determination as part of a global temperature retrieval (Smith et al. 1973), and the use of reflected sunlight around the oxygen A-band absorption for a cloud-top altitude detection (Wark and Mercer 1965). This investigation concentrates on the potential of using the oxygen A-band absorption for cloud-top pressure (height) determination for different types of clouds.

The basic idea for this type of cloud-top height detection has been known since 1961, when Yamamoto and Wark (1961) proposed it for satellite applications. The first satellite spectrographic measurements were already taken from the *Gemini 5* manned spacecraft during 22 and 28 August 1965 (Saiedy et al. 1967). This first, photographic method was replaced by a multichannel scanning radiometer for a remote sensing of cloud parameters in the mid-1970s. As part of a larger payload this instrument was successfully tested in a series of aircraft flights (Curran et al. 1981).

There are a number of investigations that used a radiance ratio, one value outside and another inside the oxygen absorption band to determine cloud-top pressure altitudes. However, the "photon penetration" problem has only been adequately dealt with by Wu (1985), who found that cloud-top pressure altitudes measured with both a lidar and a radiometer agreed well.

Corresponding author address: Dr. Jürgen Fischer, Institut für Physik, GKSS-Forschungszentrum, Postfach 1160, 2054 Geesthacht, Germany.

The goal of this study was to analyze in more detail, as has been done before, the strong dependence of the radiances within the oxygen A band upon several cloud properties, varying cloud optical thickness, surface albedo, and solar zenith angles. All these properties have to be successfully incorporated into a cloud-top height algorithm. For the development and definition of a cloud-top pressure (height) algorithm we have chosen radiative transfer modeling because of the advantage of systematically varying cloud properties and error estimates. A comparison of calculated and measured radiances as well as a test of the developed algorithms is given in an accompanying paper (part 2).

2. Methodology

Radiative transfer modeling has been shown to be of use for better understanding radiative transfer processes in atmospheres that include clouds and thus facilitates the development of remote sensing algorithms. Of course, the value of such a procedure depends on the accuracy of the radiative transfer model as well as on the use of realistic optical properties. Some new remote sensing algorithms have been developed in our group with the aid of radiative transfer modeling (Olesen and Grassl 1985; Fischer and Doerffer 1987). The principles of the radiative transfer mode and the optical properties used for this investigation are described in the following.

a. Radiative transfer model

The radiation field in the atmosphere is a function of air molecule scattering, gas absorption, atmospheric aerosol particle extinction, surface reflection, and—if present—cloud extinction. The impact of the amount and type of these molecules, particles, and droplets or crystals on the radiative transfer is expressed by only two inherent optical properties; for example, the spectral extinction and absorption coefficient. Knowing these coefficients and the corresponding phase function, the equation of radiative transfer can be solved. The calculation of radiances in optically thick media, including the effects of multiple scattering, requires methods that take considerable computer time, such as the Monte Carlo or successive order of scattering method. For this study we have chosen the matrix operator method because of its advantage to simulate not only vertically inhomogeneous but also optically thick media such as cloudy atmospheres (Fischer and Grassl 1984).

The radiative transfer equation has been solved for both azimuthally averaged and azimuthally resolved radiances, depending on the viewing angle considered. Here, for nadir radiance, which is the standard viewing direction, only the azimuthally averaged matrix operator code is used, which is much more efficient in terms of computer time.

The exponential sum-fitting technique for transmission functions (ESFT) is used to incorporate absorption by gases (Hunt and Grant 1969). For this investigation, eight expansion terms were found to be sufficient. The spectral solar emission is taken from Neckel and Labs (1981).

Reflection at the surface is assumed to be isotropic. The vertically inhomogeneous distributions of air molecules, aerosols, and cloud droplets are modeled with a number of appropriate layers. The vertical profiles of pressure, temperature, humidity, and atmospheric gases correspond to a midlatitude summer atmosphere (McClatchey 1972). It has to be mentioned that in the results section the cloud-top height is given in kilometers and not in pressure units, the latter being the quantity on which the oxygen absorption really depends. Of course, altitude values depend on the present atmospheric state. However, most publications dealing with physical cloud properties use height in kilometers for the vertical coordinate.

b. Selective absorption by water vapor and molecular oxygen

The transmission of radiation is reduced by molecular oxygen in vibration rotation absorption bands. Water vapor absorbs radiation only to a minor extent at wavelengths longer than $\lambda = 770$ nm within the considered wavelength interval $\lambda = 755$ – 775 nm. In order to study selective gaseous absorption in the radiative transfer calculations, transmission functions of O_2 and H_2O , averaged over $\Delta\lambda = 1$ nm intervals, were computed from absorption line parameters (Rothman et al. 1983). Since there is no appreciable water-vapor absorption between $\lambda = 755$ and $\lambda = 770$ nm, we neglect this feature for the radiative transfer calculations and concentrate on the effects of oxygen absorption. The transmission functions of the oxygen A-band ab-

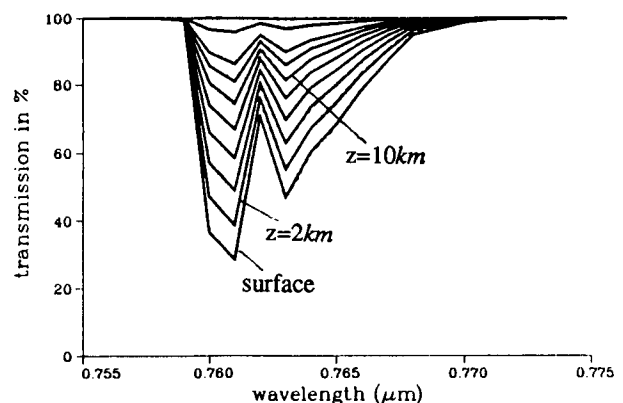


FIG. 1. Atmospheric transmission averaged over 1-nm intervals within the oxygen A-band absorption region from the top of the atmosphere to different levels: 20 (upper curve), 17, 14, 12, 10, 8, 6, 4, 2 km, and surface (lower curve); the pressure and temperature profiles correspond to a midlatitude summer atmosphere.

TABLE 1a. Exponentials k_i and related weights w_i of the used eight-term exponential sum-fitting technique; the k_i are given for certain model layers with a mean pressure level p and for $\lambda = 761$ nm.

w_i	0.1650	0.1380	0.1730	0.2310	0.0790	0.0670	0.0850	0.0620
p (hPa)	k_1	k_2	k_3	k_4	k_5	k_6	k_7	k_8
0.02	0.000227	0.000000	0.000000	0.000036	0.000011	0.000001	0.000277	0.000000
3.54	0.000036	0.000078	0.000476	0.000184	0.000082	0.000001	0.058466	0.000025
28.00	0.000000	0.000451	0.000000	0.000028	0.000150	0.000044	0.000011	0.900790
75.20	0.039172	0.054690	0.011611	0.017095	0.000042	0.008562	0.003591	1.742944
121.00	0.017527	0.345095	0.025588	0.008728	0.011391	0.001237	0.009722	3.887809
165.00	0.001029	0.242574	0.007417	0.007085	0.010100	0.015753	0.010688	1.935262
193.00	0.017484	0.247533	0.000117	0.001556	0.025499	0.000640	0.106775	2.619582
225.00	0.000007	0.019025	0.010709	0.000029	0.000010	0.000007	0.516122	4.572323
261.00	0.001347	0.000026	0.033137	0.040997	0.000011	0.000006	0.678816	4.161034
302.00	0.054165	0.000000	0.028882	0.039324	0.026001	0.021933	0.851944	4.686702
347.00	0.008119	0.000085	0.023529	0.075279	0.106299	0.047910	1.381358	1.489607
398.00	0.000001	0.005980	0.280373	0.000150	0.000001	0.000006	1.801367	2.321948
455.00	0.006416	0.511310	0.067371	0.074949	0.022778	0.009658	0.531283	6.861559
519.00	0.085720	0.374280	0.162887	0.025327	0.066872	0.000116	1.472206	19.608664
590.00	0.032520	0.477858	0.102768	0.012771	0.392243	0.092651	1.872047	107.903937
668.00	0.046716	0.553287	0.052083	0.070180	0.492138	0.134315	2.261408	122.375788
755.00	0.091331	0.680435	0.248498	0.057688	0.213349	0.125737	2.694364	95.739838
851.00	0.278352	0.764782	0.135084	0.019589	0.568263	0.066134	3.261977	114.528639
956.00	0.417596	1.121853	0.131581	0.054517	0.324430	0.083597	3.281362	158.767201

sorption within the $\lambda = 755\text{--}774$ nm domain for different pressure levels are shown in Fig. 1.

For the fulfillment of Lambert's law requirements, a set of transmission functions for different absorber masses is used to fit exponential sums that are used in the radiative transfer calculations. Since gas absorption in the atmosphere depends strongly on temperature and air pressure, we resolve the vertical temperature and pressure profile using a number of appropriate layers. The exponential sum-fitting technique has been applied to each model layer. Several layers are added

together by multiplying the transmission functions of single layers. The exponentials of each model layer are optimized, in order to describe the transmission of the total atmosphere. This is realized by minimizing the difference of the transmission functions of combined layers, estimated from these exponentials and from line-by-line calculations. For the optimization process a Simplex method was used. The extracted eight-term exponentials for the wavelengths $\lambda = 761$ and $\lambda = 763$ nm are listed in Tables 1a and 1b. The maximum root-mean-square (rms) error in our eight-term fit for the

TABLE 1b. As in Table 1a but for $\lambda = 763$ nm.

w_i	0.4060	0.0040	0.1860	0.2240	0.0330	0.0570	0.0490	0.0410
p (hPa)	k_1	k_2	k_3	k_4	k_5	k_6	k_7	k_8
0.02	0.000000	0.143014	0.000024	0.000001	0.000000	0.001463	0.000003	0.002755
3.54	0.000139	3.291554	0.000487	0.000422	0.001001	0.001472	0.000460	0.002260
28.00	0.000390	46.137873	0.001305	0.012452	1.218108	0.000199	0.000979	0.001236
75.20	0.026903	57.004235	0.030592	0.000712	2.151021	0.022156	0.024302	0.017066
121.00	0.000003	12.126551	0.010437	0.000080	4.951667	0.257282	0.009092	0.907527
165.00	0.001382	25.135436	0.000058	0.001702	1.880685	0.003524	0.254546	0.618694
193.00	0.000520	4.817480	0.020321	0.003254	3.406026	0.263587	0.099330	0.440793
225.00	0.008983	2.260212	0.042666	0.000289	3.265514	0.172818	0.099222	0.771692
261.00	0.000021	13.859593	0.020929	0.036929	4.000440	0.193199	0.225045	0.920732
302.00	0.008579	14.761213	0.014497	0.041768	4.963323	0.020954	0.559961	1.059563
347.00	0.019449	21.594534	0.003177	0.044290	53.768221	0.659480	0.004285	1.019858
398.00	0.000006	12.323808	0.040346	0.085473	6.799172	0.763651	0.075997	1.193500
455.00	0.000831	57.407231	0.003448	0.149173	33.935838	0.000461	0.705939	3.108193
519.00	0.033211	34.273600	0.108697	0.037822	9.800360	0.860555	0.253519	2.289470
590.00	0.000000	108.036370	0.197649	0.000001	17.484562	0.811775	1.198996	1.412948
668.00	0.001436	15.375963	0.368541	0.022591	5.532260	0.001857	0.737740	6.401136
755.00	0.034243	38.422609	0.272110	0.052689	18.139748	1.774399	0.003413	4.370803
851.00	0.037319	40.710006	0.294788	0.092748	10.201970	1.732948	0.628695	4.249014
956.00	0.050543	65.545519	0.390987	0.089457	13.715790	1.999898	0.712137	5.695646

transmission functions of the total atmosphere is $\epsilon < 0.00001\%$. In comparison to other studies, such as Wiscombe and Evans (1977) who quote an rms error of $\epsilon < 0.00006\%$, this procedure provides a good estimate of atmospheric absorption by gases. Furthermore, the pressure and temperature dependence of the molecular gas absorption is resolved due to the separation of the atmosphere into 20 model layers.

The temperature sensitivity of the A-band absorption was studied in some detail by Mitchel and O'Brien (1987). They found that the vertical temperature profile should be known to within 1 K, in order to retrieve the surface pressure from radiance measurements within the O₂ A band to within an accuracy of 2 hPa. Additionally, they point to the need to utilize very narrow spectral windows (1 cm⁻¹) to achieve this accuracy. However, we found a similar dependence on temperature for the cloud-top height, but for spectral intervals of $\Delta\lambda = 1$ nm. A brief analysis of the temperature dependence of the A-band absorption on the cloud-top detection will be given in section 3e.

c. Scattering by molecules and aerosols

Air molecules are small compared to the wavelength of the incoming sunlight. Hence, molecular scattering can be determined from Rayleigh theory. However, the influence of Rayleigh scattering is small for $\lambda > 0.7$ μm but is still considered here.

Atmospheric spectral turbidity variations are caused by variations of aerosol density, composition, and size distribution. Since scattering and absorption effects within the atmosphere change the spectral upwelling radiance, the evaluation of cloud properties is also affected by variations of atmospheric turbidity and aerosol type. While over wide ocean areas maritime aerosol dominates aerosol properties, over land surfaces continental or urban aerosols are present, which usually have a stronger wavelength dependence in their spectral extinction coefficients (WCP-55 1983).

In this study the spectral extinction coefficients for maritime and continental aerosols and their vertical distribution are taken from the WCP-55 report (1983). The scattering phase function is calculated by Mie theory. The range of atmospheric turbidity values chosen corresponds to horizontal visibilities at the surface between 5 and 120 km.

d. Cloud parameters

Clouds are roughly classified into water and ice clouds. For simplicity, we concentrate on water clouds for which the optical characteristics depend mainly on droplet-size distribution, total number of droplets, and vertical distribution. In a number of field campaigns various droplet-size distributions were measured. In order to consider a wide range, we selected two strongly

different cloud-droplet-size distributions with small droplets (CS) and large droplets (CB), both taken from Stephens (1979) with an effective radius of 5.25 μm (stratocumulus) and 31 μm (cumulonimbus), respectively. For the radiative transfer calculations the scattering function, the extinction coefficient, and the single-scattering albedo were all determined from Mie calculations. The minor wavelength dependence of these optical properties was also taken into account.

The geometrical thickness of the clouds was varied between 0.1 and 10 km, while the optical thickness covers a range of 0.5 to 200. The liquid-water content of the clouds can be calculated from both the optical thickness and the cloud-droplet-size distribution. However, the optical thickness of stratiform clouds is, on average, quite closely related to the geometrical thickness. Thus for clouds in the midlatitudes, the deviations from the mean relationship are not greater than 50% (Feigelson 1984). The average optical thickness δ_0 of different cloud types at fixed geometrical thickness $\Delta z_C = 1$ km varies; for stratus and stratocumulus $\delta_0 = 23$, for altostratus and altocumulus $\delta_0 = 32$, and for cumulonimbus $\delta_0 = 35$. The liquid-water content (LWC) then varies between 0.16 and 0.25 g m⁻³ at a temperature of 273 K, while the vertical LWC distribution is mainly dependent on the vertical temperature profile. In convective clouds the liquid-water content peaks in the upper third and reaches values above 1 g m⁻³ (Pruppacher 1980).

A number of cloudy atmospheres were simulated in this investigation. We distinguish between one (C1–C6) and two-layer clouds (C7–C9). Each dataset, C1–C9, was characterized by the optical and geometrical thickness, whereby the cloud-top height is gradually changed by 0.1 km between $z_{\text{max}}^{\text{top}} = 10$ km and $z_{\text{max}}^{\text{top}} = 0.1$ km (see Table 2). For the two-layer cloud cases, the upper cloud was fixed for the geometrical and optical thickness, while the cloud below was varied. In total nearly 900 cases were considered in this study.

3. Results

The first goal of this investigation was to study radiation processes in clouds with the aid of radiative transfer calculations. The contribution of different cloud properties to upward spectral radiances has to be studied in more detail, not only to understand optical phenomena in clouds, but also to get ideas for the development of remote sensing procedures. The second goal of this investigation was to define an algorithm or a procedure for detecting cloud-top pressure from upward radiances, using the effects of the oxygen A-band absorption.

First, multispectral upward radiances will be discussed to analyze the reaction of these radiances on cloud-top height. Second, different radiance ratios should provide some information the development of

TABLE 2. Cloud classes C1–C9, which differ in optical thickness δ_C , geometrical thickness Δz_C , and cloud-top height z^{top} ; both quantities are given in kilometers; minimum and maximum values are indicated.

	C1	C2	C3	C4	C5	C6	C7	C8	C9
δ_{min}	0.1	0.5	1.0	1.9	3.9	0.5	5.3	10.7	21.3
δ_{max}	1.0	4.9	9.7	19.4	38.8	48.5	48.5	97.0	194.0
Δz_{min}	0.1	0.1	0.1	0.1	0.1	0.1	1.1	1.1	1.1
Δz_{max}	1.0	1.0	1.0	1.0	1.0	10.0	10.0	10.0	10.0
$z_{\text{min}}^{\text{top}}$	0.1	0.1	0.1	0.1	0.1	0.1	0.1	0.1	0.1
$z_{\text{max}}^{\text{top}}$	10.0	10.0	10.0	10.0	10.0	10.0	10.0	10.0	10.0

cloud-top height algorithms. Furthermore, properties that affect a cloud-top height detection will be also taken into consideration.

a. Multispectral radiances

Upward radiances at the top of the atmosphere carry information about several atmospheric and surface properties. As already discussed in section 2a, the radiance depends on air molecule scattering and absorption, cloud extinction, surface albedo, and sun elevation. To demonstrate the impact of cloud-top height on the multispectral radiances in the wavelength region 0.755–0.775 μm , ten cloud-top heights ranging from $z^{\text{top}} = 1$ to $z^{\text{top}} = 10$ km were assumed for the calculations. The geometrical thickness of the clouds was fixed to $\Delta z_C = 1$ km. The cloud-droplet-size distribution corresponds to stratocumulus (CS). The spectral width of each simulated radiance is $\Delta\lambda = 1$ nm, assuming a rectangular filter function.

For the following cases, only nadir radiances are shown, the solar zenith angle $\theta_S = 35^\circ$ and the surface albedo $\alpha = 0.2$ were fixed.

Clouds with an optical thickness of 0.5 are too transparent to show significant changes in upward radiances when placed at different heights (Fig. 2a). An increase in cloud optical thickness to $\delta_C = 4.9$ and 38.8 enhances not only the total radiances but also affects the radiance differences within the oxygen A-band absorption for different cloud-top heights (Figs. 2b,c). As can clearly be seen, radiances around 0.755 μm do not depend on cloud-top height if the optical depth remains fixed.

As a first step in defining a cloud-top height algorithm, we calculate differences between radiances at $\lambda = 755$ nm and averaged radiances over wavelength intervals of: D_1 with $\Delta\lambda = 761.5 - 760.5 = 1$ nm, D_2 with $\Delta\lambda = 763.5 - 762.5 = 1$ nm, D_3 with $\Delta\lambda = 763.5 - 760.5 = 3$ nm, and D_4 with $\Delta\lambda = 768.5 - 758.5 = 10$ nm. These wavelength intervals may represent spectrometers with both different channel bandwidths and different rectangular filter functions. However, the imaging spectrometer MERIS, which is a candidate for the ESA Earth Observation Platform, will operate with a spectral sampling interval of $\Delta\lambda = 1.25$ nm (Rast 1989).

Radiance differences give an idea of the spectral signal changes due to cloud-top height variations. In Fig. 3 radiance differences are shown for different cloud-top heights and for $\delta_C = 4.9$. The highest changes are for the case D_1 because of the high absorption of oxygen around $\lambda = 761$ nm. This radiance difference $\Delta L_1 = 30.2 \text{ W m}^{-2} \text{ sr}^{-1} \mu\text{m}^{-1}$, caused by a shift of cloud-top height z^{top} from 1 to 10 km, is reduced to $\Delta L_2 = 16.7 \text{ W m}^{-2} \text{ sr}^{-1} \mu\text{m}^{-1}$ if the radiance is measured over a 10-nm spectral interval (D_4). An increase in the cloud optical thickness δ_C enhances $\Delta L_1 - \Delta L_2$.

Multispectral radiances at the top of the atmosphere for different cloud-top heights, but also for different optical thickness, are shown in Fig. 2d. The lower curve stands for $z^{\text{top}} = 1$ km and $\delta_C = 4.9$ and the upper curve for $z^{\text{top}} = 10$ km and $\delta_C = 48.5$. All other curves correspond to changes in steps of $\Delta z_C = 1$ km and $\Delta\delta_C = 4.9$. The upward radiance in the 755 nm domain is drastically changed by variations in the optical thickness of clouds. The radiance difference is no longer a linear function (nearly) of cloud-top height. Unfortunately, the radiances around $\lambda = 755$ nm and within the oxygen absorption band behave differently if the vertical distribution of the optical cloud thickness is changed. A cloud with $\delta_C = 38.8$ and $\Delta z_C = 1$ km, as well as a cloud with $\delta_C = 4.9$ and $\Delta z_C = 8$ km, cause an identical radiance value of $271.5 \text{ W m}^{-2} \text{ sr}^{-1} \mu\text{m}^{-1}$ at $\lambda = 755$ nm. At $\lambda = 761$ nm, we find for the first case $L = 127.3 \text{ W m}^{-2} \text{ sr}^{-1} \mu\text{m}^{-1}$ and for the second $L = 83.7 \text{ W m}^{-2} \text{ sr}^{-1} \mu\text{m}^{-1}$, although for both clouds $z^{\text{top}} = 8$ km is assumed (compare Figs. 2c and 2d). As a consequence of these results and for a successful cloud-top detection, we have not only to introduce the optical thickness of clouds but also—if possible—its vertical distribution.

b. Radiance ratios

As a second step in defining a cloud-top height algorithm, we calculate ratios of radiances at $\lambda = 755$ nm and wavelength intervals D_i as given in section 3a. With respect to radiance differences, nearly no dependence of the ratios on cloud-top height can be found for thin clouds in Fig. 4a. In this case the backscattered

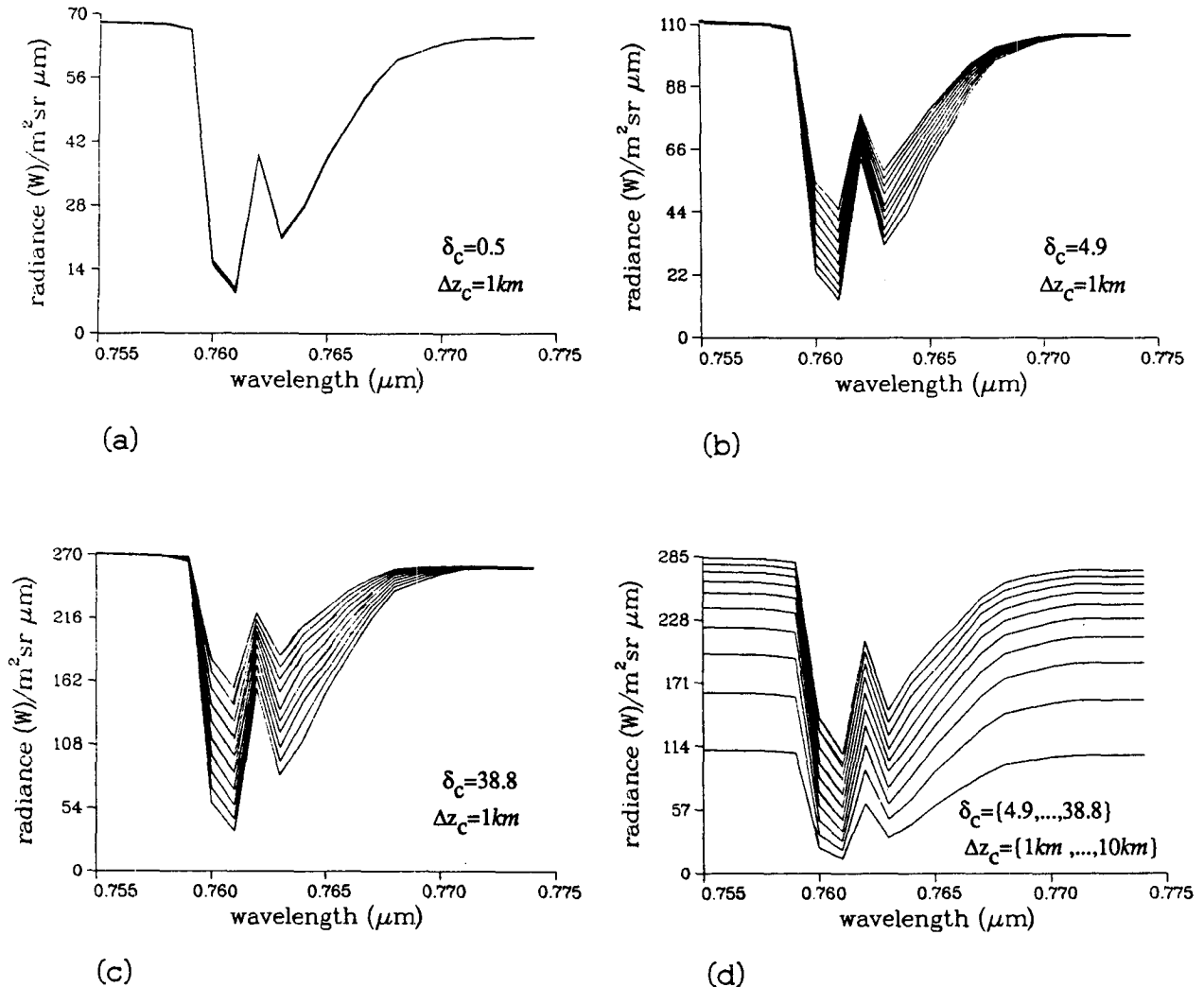


FIG. 2. Upward nadir radiances at the top of atmosphere depending on wavelength for a solar zenith angle $\theta_s = 35^\circ$ above clouds with a constant geometrical cloud thickness of $\Delta z_c = 1$ km but different cloud-top heights ranging from 10 km (uppermost curve) to 1 km: (a) for $\delta_c = 0.5$, (b) for $\delta_c = 4.9$, (c) for $\delta_c = 38.8$, and (d) in this case the cloud optical thickness δ_c and the geometrical cloud thickness Δz_c are varied between $\delta_c = 4.9$ ($\Delta z_c = 1$ km) and $\delta_c = 48.5$ ($\Delta z_c = 10$ km).

radiance originate mainly from surface reflection. For $\delta_c = 4.9$ the ratio and cloud-top height are correlated (Fig. 4b). The strongest relation is found for the 1-nm interval at $\lambda = 761$ nm. However, if δ_c varies, the quasi-linear relation between the radiance ratio and cloud-top height is nearly lost (Fig. 4c).

c. Reflectivity

The reflectivity or albedo, the ratio of upward and downward flux, at the top of the atmosphere is a measure of the backscattered radiation and also helps in understanding the portion of radiation backscattered within the absorption region. In Fig. 5, reflectivity depending on δ_c is shown for $\lambda = 755$ nm. There is no

linear relation between the two quantities, but a saturation tendency for large δ_c and cloud height has only a negligible influence. The larger number of cloud droplets in a CS cloud, assuming a fixed optical thickness for both droplet-size distributions, causes an enhanced reflectivity, because then radiation does not penetrate so deeply into a cloud.

d. Other properties influencing cloud-top height detection

One consequence of the results discussed so far is that a cloud-top height algorithm has to consider not only radiance ratios with intervals inside and outside the oxygen band, but also the photon penetration into

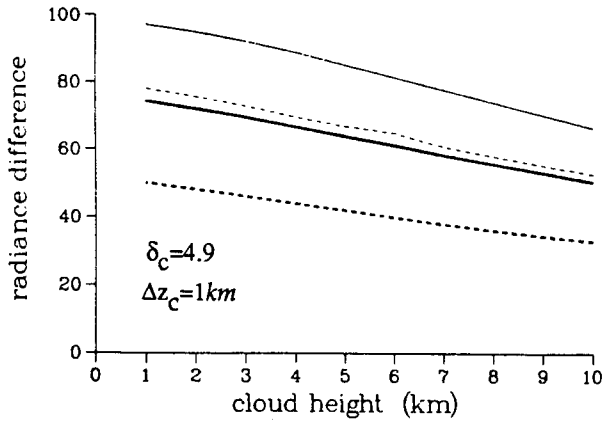
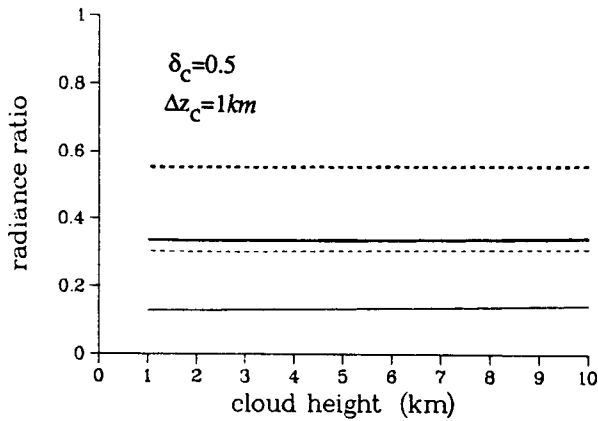


FIG. 3. Differences of nadir radiances $\Delta L = L_{\lambda=755 \text{ nm}} - L_{\Delta\lambda_i}$ ($\text{W m}^{-2} \text{sr}^{-1} \mu\text{m}^{-1}$) above a cloud with $\delta_c = 4.9$ as a function of cloud-top height, $\theta_s = 35^\circ$; four different spectral intervals $\Delta\lambda_i$ are considered within the absorption band: $\Delta\lambda_1 = 761.5 - 761.5 \text{ nm}$ (—), $\Delta\lambda_2 = 763.5 - 762.5 \text{ nm}$ (---), $\Delta\lambda_3 = 763.5 - 760.5 \text{ nm}$ (-·-·-), and $\Delta\lambda_4 = 768.5 - 758.5 \text{ nm}$ (···).

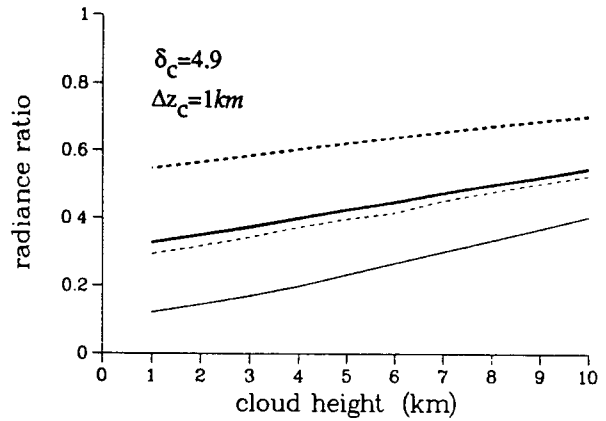
the clouds has to be matched adequately. To complicate matters further the vertical distribution of the optical thickness, cloud-droplet-size distribution, sun elevation, and surface albedo also affect the cloud-top height detection.

1) OPTICAL THICKNESS AND ITS VERTICAL DISTRIBUTION

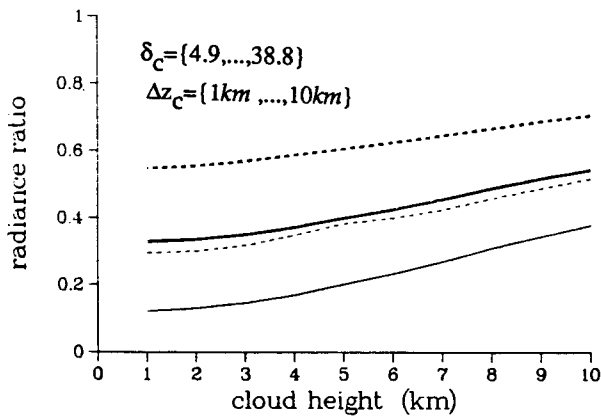
As already stated in section 3a, the vertical distribution of cloud optical thickness affects the radiances differently within and outside the oxygen absorption band. While radiances around $\lambda = 755 \text{ nm}$ depend only on total optical thickness, radiances within the absorption band are also related to the vertical distribution of liquid water. Photons that penetrate into deeper cloud layers have a higher probability of becoming absorbed. Thus the ratio of radiances at $\lambda = 761$ and $\lambda = 755 \text{ nm}$ is smaller for clouds with a larger geometrical thickness but the same optical



(a)



(b)



(c)

FIG. 4. Radiance ratio $L_{\Delta\lambda_i}/L_{\lambda=755 \text{ nm}}$ as a function of cloud-top height for the same spectral intervals $\Delta\lambda_i$ as in Fig. 3: (a) for $\delta_c = 0.5$, (b) for $\delta_c = 4.9$, and (c) for varying δ_c and Δz_c between $\delta_c = 4.9$ ($\Delta z_c = 1 \text{ km}$) and $\delta_c = 48.5$ ($\Delta z_c = 10 \text{ km}$).

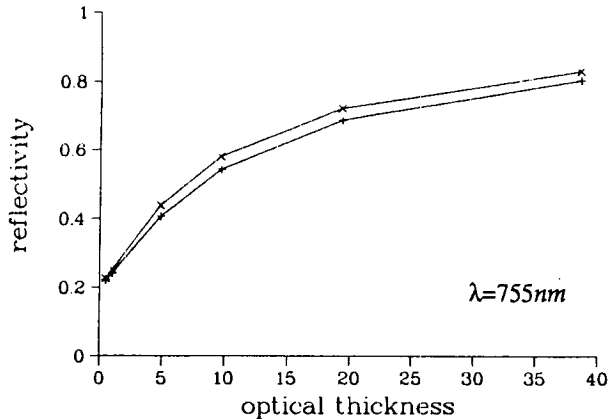


FIG. 5. Reflectivity at the top of atmosphere for $\lambda = 755$ nm depending on cloud optical thickness δ_C ; the cloud is $z^{\text{top}} = 6$ km high and has a geometrical thickness of $\Delta z_C = 1$ km, $\theta_S = 35^\circ$. Two different cloud-droplet-size distributions with mean radii $\bar{r} = 5.25$ μm (\times) and $\bar{r} = 31$ μm ($+$) are assumed.

thickness and height. Since there is no procedure available to date that can retrieve the vertical distribution of liquid water from near-infrared radiance measurements, the accuracy of a cloud-top height algorithm will also depend on the natural vertical variations of LWC.

Typically on the macroscale, the cloud-water content increases with height above the cloud base, assumes a maximum in the upper half of the cloud and decreases rather quickly toward the cloud top (Pruppacher 1980). Also, the liquid-water content of different cloud types such as altostratus and altocumulus, stratus and stratocumulus, and cumulonimbus differ only by a factor of 2 as long as the temperature does not exceed 280 K (Feigelson 1984). Following these statements, the variations of liquid-water content and its vertical distribution are limited and therefore an introduction of standard liquid-water content profiles for different regions and seasons within the algorithm may enhance the accuracy of retrieved cloud-top heights. However, multilayer clouds are the most difficult cases for upper layer cloud-top detection. The optical properties of underlying clouds significantly affect the multispectral radiances of high clouds, as will be seen for the application of our cloud-top procedures in section 3e and 3f.

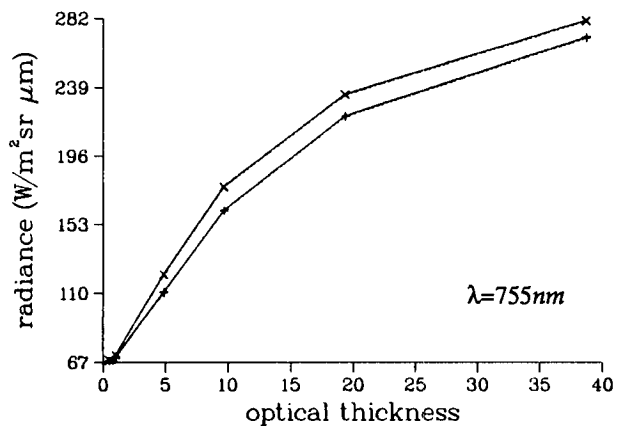
2) CLOUD-DROPLET-SIZE DISTRIBUTION

Water clouds are often sufficiently characterized by their cloud-droplet-size distribution and liquid-water content. Both parameters determine the optical thickness. The upward radiances at $\lambda = 755$ nm are slightly affected by the size distribution (Fig. 6a). The high number of smaller droplets in CS clouds increase

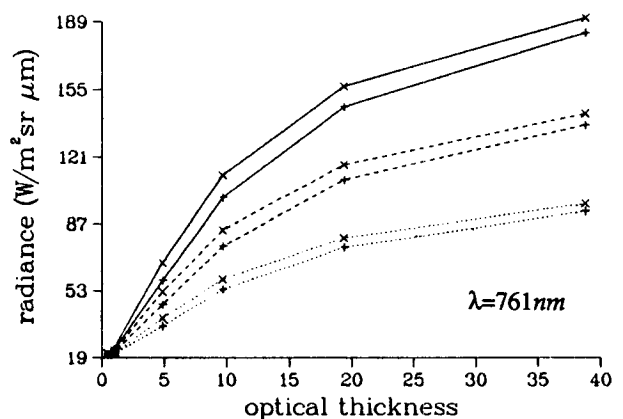
backscattering. The impact of different cloud-top heights on the upward radiances at $\lambda = 755$ nm is nearly negligible. Within the oxygen absorption bands, the upward radiance depends additionally on cloud-top height and is more strongly modified by different cloud types, in this instance characterized by different cloud-droplet sizes (Fig. 6b).

3) SUN ELEVATION

The amount of backscattered radiation is also dependent on sun elevation or solar zenith angle, mainly because of an increase of relative air mass for lower angles. In Fig. 7 the ratio of upward radiances at $\lambda = 761$ and $\lambda = 755$ nm is shown for three cloud-top

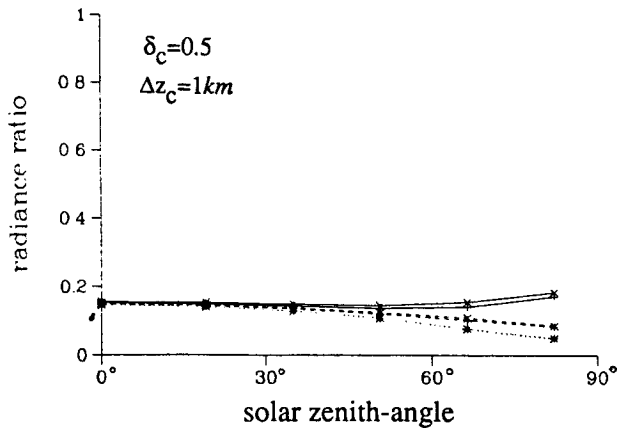


(a)

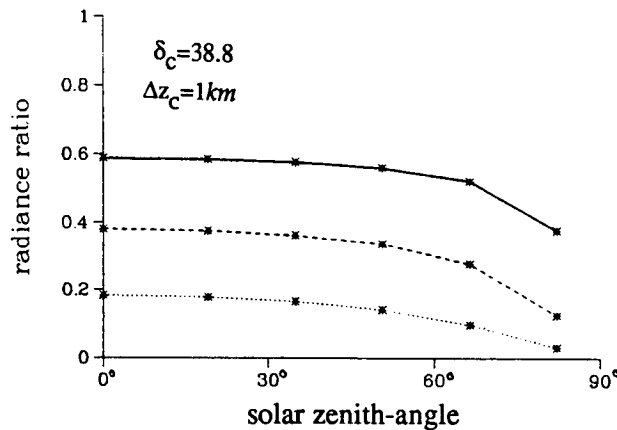


(b)

FIG. 6. Upward nadir radiances at the top of the atmosphere depending on cloud optical thickness δ_C using the same optical properties as in Fig. 5, but for three different cloud-top heights $z^{\text{top}} = 2$ km (\cdots), $z^{\text{top}} = 6$ km ($---$), and $z^{\text{top}} = 10$ km ($---$): (a) for $\lambda = 755$ nm, and (b) for $\lambda = 761$ nm.



(a)



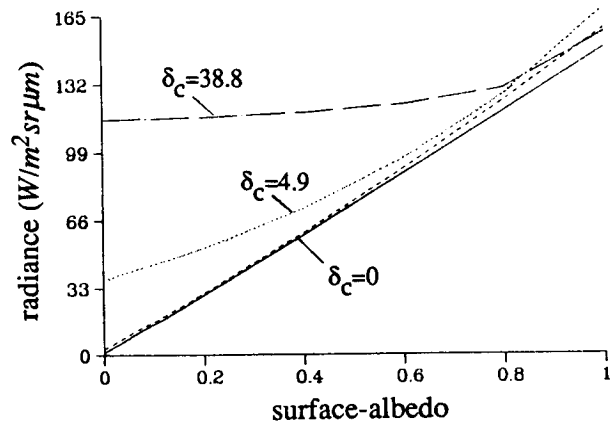
(b)

FIG. 7. Radiance ratio $L_{\lambda=761 \text{ nm}}/L_{\lambda=755 \text{ nm}}$ for clouds with different cloud-top heights according to Fig. 6 as a function of θ_S : (a) for $\delta_C = 0.5$, and (b) for $\delta_C = 38.8$.

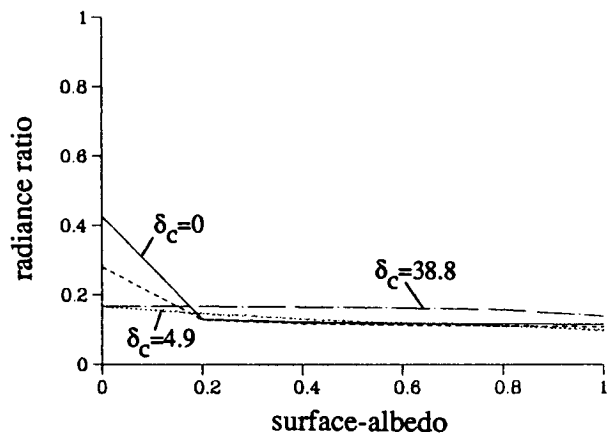
heights as a function of solar zenith angle θ_S . For optically thin clouds ($\delta_C = 0.5$) no significant change for different cloud heights is found, as long as θ_S is below 50° (Fig. 7a). At higher θ_S absorption increases so that a distinction between different cloud heights becomes obvious. A comparison between clouds with $\delta_C = 0.5$ (Fig. 7a) and $\delta_C = 38.8$ (Fig. 7b) shows a significant change in the behavior for the dependence on solar zenith angle. While for optically thicker clouds the radiance ratios decrease with solar zenith angle for all cloud heights, the thinner clouds increase the ratio with increasing θ_S for high clouds. This behavior is caused by the competitive effects of increased scattering by clouds and increased oxygen absorption for lower sun elevations.

4) SURFACE ALBEDO

Surface albedo also affects radiances above clouds. Of course, the contribution of the underlying surface depends on the optical thickness of the clouds. Differences of radiances $L_{\lambda=755 \text{ nm}} - L_{\lambda=761 \text{ nm}}$ depend linearly on surface albedo for cloud-free atmospheres (Fig. 8a). Transparent clouds behave similarly. Even clouds with an optical thickness of $\delta_C = 4.9$ are still affected by surface reflection. However, the ratio $L_{\lambda=761 \text{ nm}}/L_{\lambda=755 \text{ nm}}$ shows only important effects of surface albedo for $\alpha < 0.2$ and $\delta_C < 4.9$ (Fig. 8b). Above a black surface ($\alpha = 0$) the ratio $L_{\lambda=761 \text{ nm}}/L_{\lambda=755 \text{ nm}}$ reaches values above 0.4 because of the influence of molecular



(a)



(b)

FIG. 8. (a) Differences of nadir radiances $\Delta L = L_{\lambda=755 \text{ nm}} - L_{\lambda=761 \text{ nm}}$ for clouds with fixed cloud-top heights $z^{\text{top}} = 2 \text{ km}$ and $\delta_C = 0$ (—), $\delta_C = 0.5$ (---), $\delta_C = 4.9$ (· · ·), and $\delta_C = 38.8$ (- · -) as a function of surface albedo, $\theta_S = 35^\circ$. (b) As in (a), but for the radiance ratio $L_{\lambda=761 \text{ nm}}/L_{\lambda=755 \text{ nm}}$.

scattering, which acts at all levels within the atmosphere. This effect decreases rapidly when the cloud optical thickness increases. Nevertheless, many surfaces and clouds fall into this category. Therefore a discrimination between thin clouds and surfaces has to be made.

e. Cloud-top height detection from one radiance ratio

For a cloud-top algorithm we have to consider all the properties that act on the ratio of radiances within and outside the oxygen absorption band. The most important property is the optical thickness δ_C of a cloud. Sun elevation is also important but is easily given by the local time, season, and geographical latitude of a satellite overpass. Even the surface albedo can be considered within the algorithm if estimated from measurements obtained during cloud-free overpasses. Following the above sensitivity tests, we propose an algorithm for cloud-top height:

$$z_{*}^{\text{top}} = \frac{D}{R_{\text{Sat}}} + AR_{\text{Sat}} \left[B \frac{L_{\text{max}}}{L_{\text{Sat}}} + \exp \left(C \frac{L_{\text{max}}}{L_{\text{Sat}}} \right) \right]. \quad (1)$$

Here R_{Sat} is the ratio of the radiances measured at $\lambda = 755 \text{ nm}$ and $\lambda = 761 \text{ nm}$. L_{max} is the possible maximum upward radiance at $\lambda = 755 \text{ nm}$ reflected by clouds that depends on the solar zenith angle (Table 3). Also L_{Sat} is the radiance that is actually measured at $\lambda = 755 \text{ nm}$. The ratio $L_{\text{max}}/L_{\text{Sat}}$ provide information concerning the cloud optical thickness δ_C , and thus enable us to correct for photon penetration effects. The coefficients A , B , C , and D depend on the ensemble of clouds considered and are determined using a minimization procedure (Table 3).

This empirical equation describes the nonlinear relationship between the radiance ratios for different conditions and different cloud-top heights quite well. Before we chose Eq. (1) as the best predictor for cloud heights, we analyzed a number of relationships, all of which include a linear and a nonlinear term and which are necessary to describe the dependency of cloud-top height on the radiance ratio and cloud optical thickness

TABLE 3. Maximum upward nadir radiances L_{max} ($\text{Wm}^{-2} \text{sr}^{-1} \mu\text{m}^{-1}$) and the coefficients A , B , C , and D of Eq. (1) depending on θ_s for the cloud cases C1–C5; for the second line with $\theta_s = 35^\circ$ all cloud cases C1–C9 are considered. Here F_{min} is the error variance of the best fit.

θ_s	L_{max}	A	B	C	D	F_{min}
0.0°	404	14.548	-0.067	0.219	-0.258	39.8 m
19.1°	378	14.394	-0.043	0.210	-0.236	32.7 m
35.0°	328	14.194	0.009	0.186	-0.185	20.5 m
*35.0°	328	30.363	-0.527	0.291	-0.143	3111 m
50.7°	254	14.691	0.019	0.172	-0.110	13.8 m
66.4°	160	17.391	-0.077	0.192	-0.023	52.2 m
82.1°	55	35.817	0.226	-0.314	0.027	61.1 m

that is introduced by the ratio $L_{\text{max}}/L_{\text{Sat}}$. The criterion for the best algorithm was the minimum error in cloud-height detection.

For one-layer clouds with constant geometrical cloud thickness $\Delta z_C = 1 \text{ km}$ (C1–C5 of Table 2), the coefficients used in Eq. (1) are contained in Table 3. A comparison between prescribed z^{top} and estimated cloud height z_{*}^{top} is shown in Fig. 9a. The ratio R_{Sat} itself scatters much more than z_{*}^{top} relative to z^{top} so that a cloud-height detection, considering only this ratio, would definitely fail (Fig. 9a). Furthermore, the result of Eq. (1) is not acceptable for $\delta_C \leq 0.5$ (C1). The average error of the retrieved cloud heights is $\epsilon = 91 \text{ m}$ for the best case at $\theta_s = 35.0^\circ$ and mean optical thickness (C3 in Table 4). The cloud-top height can be estimated to within 150 m, if $\text{LWC} > 0.1 \text{ g m}^{-3}$ and $\delta_C > 5$. Optically thin clouds can be detected more accurately at lower sun elevations, as already indicated in section 3d.3. Up to now only the errors due to the algorithm were discussed. Normally distributed measurement errors for the upward radiances reduce the accuracy further (Table 4). For cloud cases C2–C5, a large error of 5% increases the average cloud-height error from 131 to 469 m.

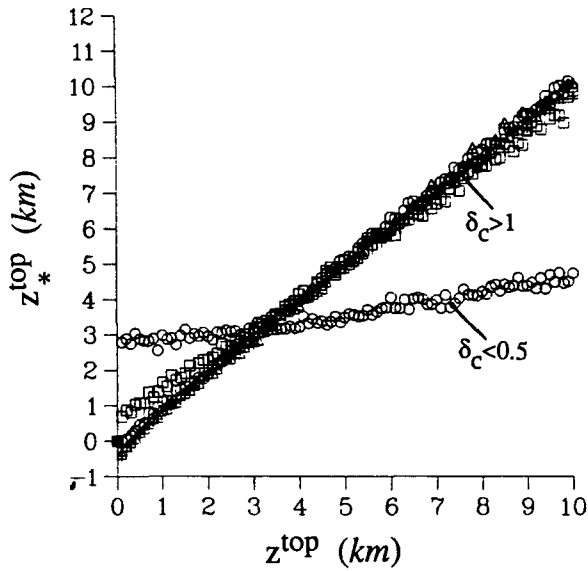
When different vertical liquid-water distributions are introduced, as for cases C6–C9 of Table 2, new coefficients A , B , C , and D follow, as long as the criterion of a minimum error for all cloud cases is also applied. Thus, the algorithm or the coefficients become dependent on the cases considered (See Table 3 for $\theta_s = 35.0^\circ$ and $\theta_s = *35.0^\circ$). The errors of the retrieved cloud heights now exceed 1000 m for most of the cases. The detection of clouds with $\delta_C \leq 1$ and multilayer clouds fails totally, and for all other cloud cases the estimation errors are also not acceptable (Fig. 9b). A separation into a class consisting of two-layer clouds enhances the accuracy.

As a consequence, in order to retrieve cloud heights from only one radiance ratio at tolerable errors, we either have to introduce the vertical distribution of the cloud liquid water into the detection procedure or have to apply different algorithms for one- and two-layer clouds.

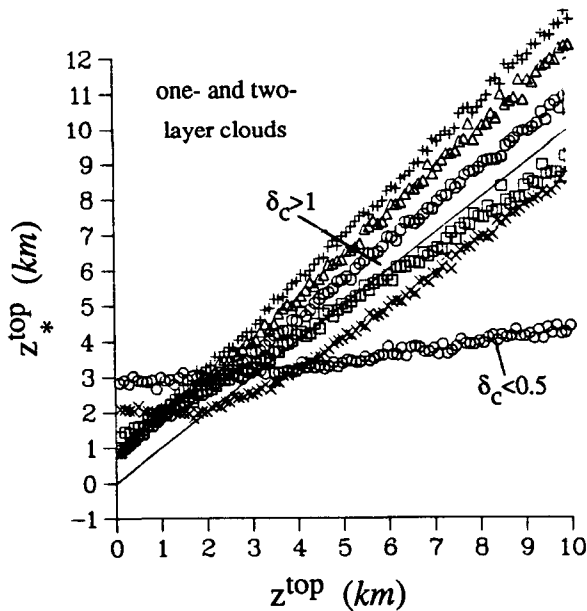
The temperature sensitivity of the O_2 A-band absorption is an additional source of error in cloud-top detection. Our estimate of a change in retrieved cloud-top height from Eq. (1) due to an increase of 1 K is about $\Delta z_{*}^{\text{top}} = 15 \text{ m}$ for a mean cloud-top height $z_{*}^{\text{top}} = 1 \text{ km}$ and a solar zenith angle $\theta_s = 35^\circ$. Thus, the vertical temperature profile should be considered and, at least, taken from climatology tables or better from actual vertical soundings.

f. Cloud-top height detection from multispectral radiances

The above algorithm for cloud-top height detection was based on radiances at only two wavelengths. The



(a)



(b)

FIG. 9. (a) Estimated cloud heights z_{*}^{top} using Eq. (1) versus prescribed values z^{top} for only one-layer clouds; clouds with an optical thickness $\delta_c < 0.5$ are indicated (O), all other symbols stand for clouds with $\delta_c > 1$ (see C1–C5 in Table 2), $\theta_s = 35^\circ$. The assumed relative radiance error is $\epsilon = 1\%$. (b) As in (a), but for one- and two-layer clouds C1–C9 according to Table 2.

effects of varying δ_c are accounted for by also using the absolute radiances at $\lambda = 755$ nm. The restriction of this technique is that varying liquid-water profiles or multilayer clouds cannot be successfully handled

TABLE 4. Errors in cloud height detection in meters; C1, . . . , C5 stands for different classes of cloud variations according to Table 2; normally distributed measuring errors ϵ are assumed.

θ_s	ϵ	C1	C2	C3	C4	C5
0.0°	0%	2377	357	106	142	129
19.1°	0%	2353	313	103	131	115
35.0°	0%	2277	228	91	108	98
35.0°	1%	2299	257	121	137	136
35.0°	5%	2416	607	393	446	429
50.7°	0%	2016	162	95	105	119
66.5°	0%	1435	293	293	310	320
82.2°	0%	1112	1030	1095	1144	1171

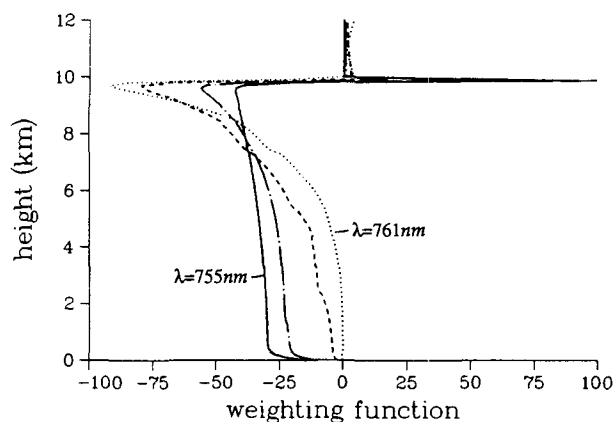
and, thus, the accuracy of a cloud-top height algorithm will depend on the natural variations in the vertical distribution of LWC. Since there is no validated procedure to date that can be used to retrieve the vertical distribution of liquid water from near infrared radiance measurements, we first look at the information content of LWC profiles that can be obtained from multispectral radiances within the wavelength region $\lambda = 755\text{--}770$ nm. As a second step we discuss an inverse technique that uses a number of different spectral radiances for cloud-top detection.

1) WEIGHTING FUNCTIONS WITHIN THE O₂ A-BAND ABSORPTION

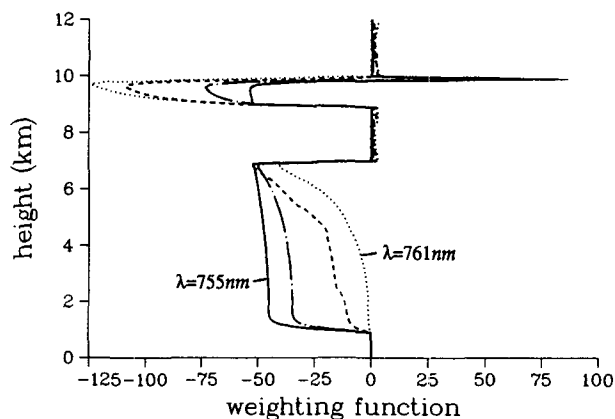
As already discussed earlier, the vertical distribution of cloud optical thickness affects the radiances differently inside and outside of the oxygen absorption band. While radiances around $\lambda = 755$ nm only depend on total optical thickness, radiances within the absorption band are also related to the vertical distribution of liquid water. Thus, the ratio of radiances at $\lambda = 755$ and $\lambda = 761$ nm is smaller for clouds with a larger geometrical depth but the same optical thickness and height. However, the oxygen A-band absorption varies characteristically within the wavelength domain $\lambda = 755\text{--}770$ nm, and thus, depending on wavelength, radiation penetrates to different depths within clouds. Therefore, multispectral upward radiances should also carry information on the vertical profile of the volume scattering coefficient that is linearly related to the liquid-water content and mean size of the cloud droplets.

The information content of upward radiances at different wavelengths within the O₂ A-band absorption is studied with the aid of weighting functions defined by $\delta L^- / \delta z$. These functions are characteristic for different wavelengths, such as shown in Figs. 10a and 10b. Within the nonabsorbing wavelength region ($\lambda = 755$ nm), the contribution to the radiances at the top of the atmosphere originates with nearly the same intensity from all layers of the cloud, while radiances within the O₂ absorption band, i.e., at $\lambda = 761$ nm, are mainly

caused by scattering in the upper cloud layers. Thus, the radiance measured above a cloud originates at different depths of the cloud depending on the amount of O_2 absorption. However, the strong peak of $\delta L^-/\delta z$ at the cloud top, as is obvious at 10 km for both cloud cases, stems from the unisotropic radiance field at upper cloud layers and the approximately isotropic radiation within deeper cloud layers. In this case the isotropic radiation surmounts the nadir radiance at the cloud top. Such a peak does not exist at the top of the lower cloud of the two-layer cloud case (Fig. 10b); this is because the downwelling radiation field is near to isotropy below the upper cloud. For both cloud cases the weighting functions show a similar characteristic for



(a)



(b)

FIG. 10. (a) Weighting functions defined by $\delta L^-/\delta z$ depending on height for $\lambda = 755$ nm (—), $\lambda = 761$ nm (\cdots), $\lambda = 764$ nm (---), and $\lambda = 767$ nm (- · -); the cloud extends from the surface to 10 km and is assumed to be vertically homogeneous with a total cloud optical thickness $\delta_c = 200$, $\theta_s = 35^\circ$. (b) As in (a), but for a two-layer cloud with a total cloud optical thickness $\delta_c = 140$.

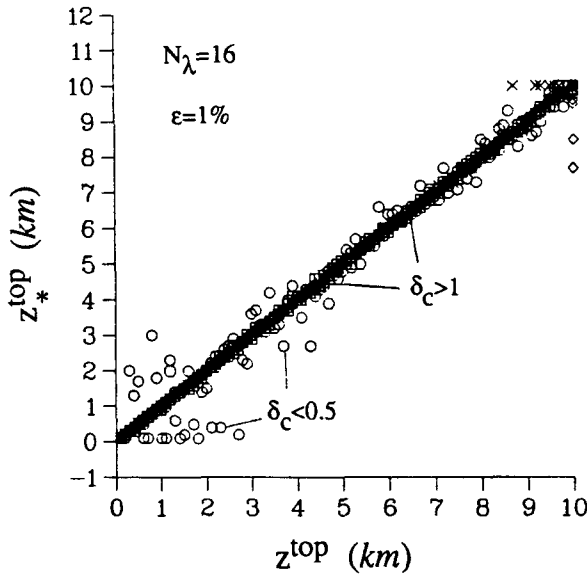
all wavelengths. The next step is the choice of an adequate method for cloud-top height detection, which considers a certain number of multispectral radiances.

2) INVERSE MODELING TECHNIQUE FOR CLOUD HEIGHT DETECTION

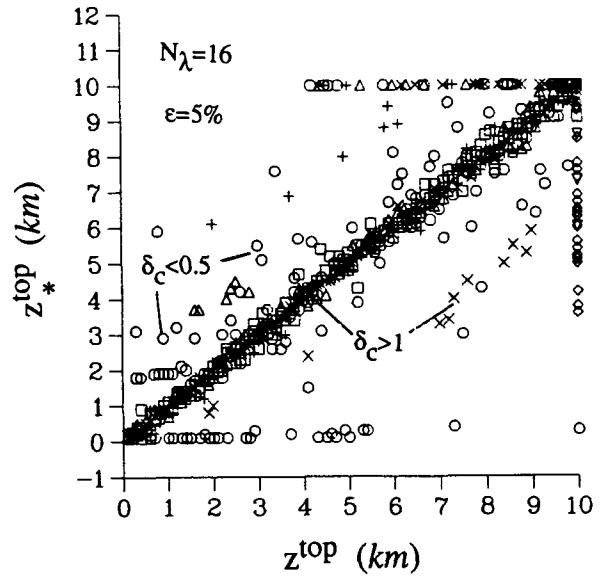
Inverse modeling procedures have already been successfully used for the retrieval of substance concentrations in ocean water from multispectral measurements (Fischer and Doerffer 1987). The basic idea of such a technique is to minimize an error function, such as the χ^2 function. The input for this function is both measured and simulated in multispectral upward radiances. The optical properties of an appropriate radiative transfer model are varied until an optimal fit is reached. Since the radiative transfer calculations for a cloudy atmosphere would consume too much computer time, we chose for this investigation a look-up table technique. The table contains numerous calculated multispectral radiances, optical properties, and cloud heights, thereby covering many possible variations in the atmosphere. For a first test of this procedure we simulated the "measured" multispectral upward radiances, in order to analyze the potential of such a method under well-defined conditions.

We applied the look-up table technique to a set of different clouds, such as summarized in the cases C1–C9 of Table 2. If we assume a normally distributed error of $\epsilon = 1\%$, the corresponding mean deviations of estimated and prescribed cloud heights are within 50 m for most of the considered cloud cases (Table 5 and Fig. 11a). The cloud-top height of thin clouds with $\delta_c \leq 0.5$ (C1) is difficult to detect, even when 16 multispectral radiances are used. However, for this cloud-top height detection method we also find that optically thin clouds may be detected more accurately at lower sun elevations, as already seen in section 3d.3. The signal-to-noise ratio of a radiometer may, however, act in the opposite direction. The above procedure took $N_\lambda = 16$ radiance measurements at different wavelengths by comparing $\lambda = 755$ and $\lambda = 758$ with $\lambda = 772$ nm with $\Delta\lambda = 1$ nm and a rectangular filter function.

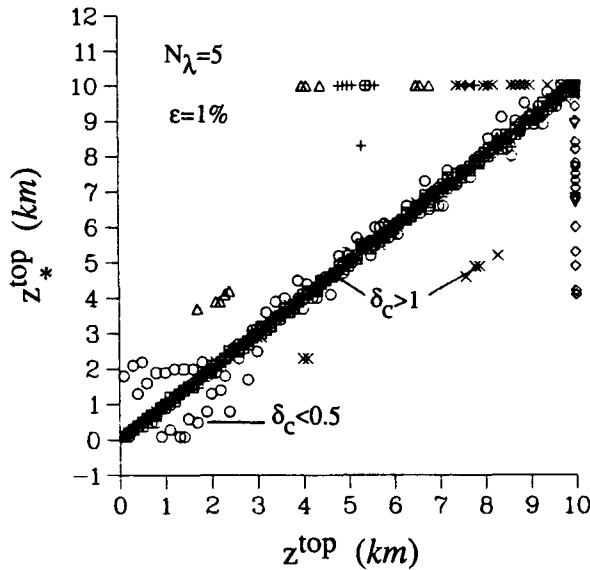
A reduction in the number of channels N_λ used slightly affects the accuracy of the estimated cloud-top heights (Table 6a). The average estimation error in cloud-top height of all cloud cases (C1–C9) is 82 m for $N_\lambda = 16$ and 269 m for $N_\lambda = 5$ and $\epsilon = 1\%$ (Table 6a and Fig. 11c). Although the error increases by a factor of three when N_λ is decreased, the accuracy of the estimated cloud-top height is not necessarily increased, because the significance of a measurement is proportional to $1/N_\lambda$. Here, we found a reduction in the rms errors in some cases when the number of channels were reduced from seven to five (see Tables 6a and 6b). In those cases the number of channels used increased the errors, but did not increase the infor-



(a)



(b)



(c)

FIG. 11. (a) Estimated cloud heights z_*^{top} using the inverse modeling technique for $N_\lambda = 16$ wavelengths versus prescribed values z^{top} ; clouds with an optical thickness $\delta_c < 0.5$ are indicated (O). All other symbols stand for clouds with $\delta_c > 1$. The assumed error for the radiances is $\epsilon = 1\%$, and the solar zenith angle is $\theta_s = 35^\circ$. (b) As in (a), but for $\epsilon = 5\%$. (c) As in (a), but for only $N_\lambda = 5$ wavelengths and $\epsilon = 1\%$.

mation content of the multispectral radiances. For $N_\lambda = 5$ we used $\lambda = 755, 761, 763, 765,$ and 767 nm. It is important to note that if Tables 5 and 6 contain no deviation from the prescribed cloud height, for instance columns C8 and C9 in Table 5, this only indicates that the correct value in the look-up table (with $\Delta z^{\text{top}} = 100$ m separation) has been found for all clouds in this class.

An error in the radiance measurements significantly affects the accuracy of the cloud-top retrieval. An increase from $\epsilon = 1\%$ to $\epsilon = 5\%$ reduces the accuracy of the cloud-top height estimation with $N_\lambda = 16$ to roughly 500 m (Table 6b and Fig. 11b). A reduction of N_λ further reduces the accuracy of the estimated cloud-top height. However, new array spectrometers measure radiances at different wavelengths more accurately. A

TABLE 5. Deviations of estimated cloud heights from prescribed values in meters for cloud cases C1, . . . , C9 and a normally distributed radiance error $\epsilon = 1\%$.

θ_s	C1	C2	C3	C4	C5	C6	C7	C8	C9
0.0°	731	51	37	34	27	28	49	0	0
19.1°	642	49	36	34	27	28	49	0	0
35.0°	492	43	43	32	25	53	49	0	0
50.7°	201	33	37	47	22	61	39	0	0
66.5°	88	26	32	22	20	16	21	0	0
82.2°	54	21	19	31	15	10	2	0	0

relative error of $\epsilon < 1\%$ is not too optimistic. A calibration of absolute radiances is, of course, more difficult, but errors below 5% are likely to be achieved.

4. Discussion and conclusions

This investigation has focused on the retrieval of cloud-top height from multispectral measurements in the oxygen A-band absorption region. We used a radiative transfer model because of the advantage of a systematic analysis of possible perturbing parameters, which affect a cloud-height detection. However, the results are only transferable to real atmospheric conditions as far as the assumption of a vertically inhomogeneous but plane-parallel atmosphere-cloud system and the used optical properties are correct. The variations of cloud optical properties covering a wide range were taken from observations. The range $0.1 \leq \delta_C \leq 197$ for optical thickness and $0.1 \leq z^{top} \leq 10$ km for cloud height try to encompass most of the layer cloud cases occurring in the atmosphere.

Our major findings with respect to perturbing effects for cloud-height detection are:

1) The most important quantity is the cloud optical thickness δ_C , which strongly affects the ratio of radiances at $\lambda = 761$ and $\lambda = 755$ nm. However, the radiance outside the absorption band is well correlated to δ_C .

2) The vertical distribution of liquid-water content determines the radiances in the absorption band, also for optically thick clouds. Therefore these radiances must contain some information on the liquid-water content profile.

TABLE 6a. As in Table 5, but for $\theta_s = 35^\circ$; N_λ wavelengths and $\epsilon = 1\%$.

N_λ	C1	C2	C3	C4	C5	C6	C7	C8	C9
16	492	43	43	32	25	53	49	0	0
7	556	60	61	125	47	224	179	0	0
5	512	65	56	103	76	284	178	37	0
2	405	49	105	407	455	398	526	76	0

TABLE 6b. As in Table 5, but for $\theta_s = 35^\circ$; N_λ wavelengths and $\epsilon = 5\%$.

N_λ	C1	C2	C3	C4	C5	C6	C7	C8	C9
16	1791	238	467	522	540	613	877	81	0
7	2430	384	778	1052	1057	838	969	150	0
5	2282	362	683	1136	1217	824	1014	209	64
2	2315	416	925	1611	1585	1163	1183	381	63

3) The influence of varying cloud-droplet-size distributions is of minor importance.

4) The surface albedo has to be known for clouds with $\delta_C < 5$.

5) Sun elevation acts differently on the radiances within and outside the absorption band, but may easily be considered.

6) The vertical temperature profile has to be considered.

The results of this sensitivity analysis led to two cloud-top height detection procedures.

- The first procedure involves an algorithm for two radiances at $\lambda = 755$ and $\lambda = 761$ nm with $\Delta\lambda = 1$ nm and one-layer clouds. The effects of varying δ_C could be handled well. The cloud height is determined with an accuracy better than 200 m at a given mean vertical liquid-water content and for $\delta_C > 5$.

- The second procedure encompasses an inverse modeling technique, based on look-up tables containing upward radiances around the oxygen A-band absorption with a resolution of $\Delta\lambda = 1$ nm. This technique is sufficiently accurate for all cases including two cloud layers and varying liquid-water profiles if 16 wavelengths are used. The rms error of retrieved cloud heights is mostly smaller than 50 m if a normally distributed error of 1% for the radiances is assumed. A reduction of the number of wavelengths from 16 to 5 increases the error by slightly more than a factor of 2.

Aside from this first success, further theoretical and experimental investigations have to show whether other properties limit cloud-height detection from passive radiance measurements. These investigations should include:

- the simulation of azimuthally resolved radiances inside and outside the oxygen A-band absorption for strongly off-nadir remote sensing;
- variations of liquid-water profiles; and
- the effects of the three-dimensionality of clouds.

A first verification of the proposed cloud-top detection technique is given in part 2 of this paper, where simultaneous lidar and multispectral radiance measurements are evaluated for cloud-top heights over stratocumulus clouds (Fischer et al. 1991).

Following the results of this study, only the use of highly resolving spectrometers will give the necessary information for a retrieval of physical and microphysical cloud properties. Recent developments of array spectrometers promise to resolve the spectral region between 0.4 and 1.0 μm to within $\Delta\lambda < 2$ nm. For an earth observation system, ESA proposed a medium-resolution imaging spectrometer (MERIS) whose specifications could fulfill such requirements.

REFERENCES

- Cox, S. K., 1980: Radiation characteristics of clouds in the solar spectrum. *Clouds: Their Formation, Optical Properties, and Effects*. P. Hobbs and A. Deepak, Eds., 93–185.
- Curran, R. J., H. L. Kyle, L. R. Blaine, J. Smith and T. D. Clem, 1981: Multichannel scanning radiometer for remote sensing cloud physical parameters. *Rev. Sci. Spectrum*, **52**, 1546–1555.
- , and M. L. Wu, 1982: Skylab near-infrared observations of clouds indicating supercooled liquid water droplets. *J. Atmos. Sci.*, **39**, 635–647.
- Feigelson, E. M., 1984: *Radiation in a cloudy atmosphere*. Reidel.
- Fischer, J., and H. Grassl, 1984: Radiative transfer in an atmosphere-ocean system: An azimuthally dependent matrix-operator approach. *Appl. Opt.*, **23**, 1032–1039.
- , and R. Doerffer, 1987: An inverse technique for remote detection of suspended matter, phytoplankton and yellow substance from CZCS measurements. *Adv. Space Res.*, **7**, 21–26.
- , W. Cordes, A. Schmitz-Peiffer, W. Renger and P. Mörl, 1991: Detection of cloud-top height from backscattered radiances within the oxygen A Band. Part 2: Measurements. *J. Appl. Meteor.*, **30**, 1260–1267.
- Hunt, G., and I. Grant, 1970: Discrete space theory of radiative transfer and its application to problems in planetary atmospheres. *J. Atmos. Sci.*, **26**, 963–972.
- McClatchey, R. A., R. W. Fenn, J. A. Selby, F. E. Volz and J. S. Garing, 1972: Optical properties of the atmosphere. AFCRL-72.0497, Environmental Research Papers, No. 411.
- McCleese, D. J., and L. S. Wilson, 1976: Cloud top heights from temperature sounding instruments. *Quart. J. Roy. Meteor. Soc.*, **102**, 781 pp.
- Mitchel R. M., and D. M. O'Brien, 1987: Error estimates for passive satellite measurements of surface pressure using absorption in the A-band of oxygen. *J. Atmos. Sci.*, **44**, 1981–1990.
- NASA, 1986: MODIS—instrument panel report. *Earth Observation System, Vol IIb*.
- Neckel, H., and D. Labs, 1981: Improved data of solar spectral irradiance from 330 to 1250 μm . *Sol Phys.*, **74**, 231–249.
- Ohring, G., and S. Adler, 1978: Some experiments with a zonally averaged climate model. *J. Atmos. Sci.*, **35**, 186–205.
- Olesen, F.-S., and H. Grassl, 1985: Cloud detection and classification over oceans at night with NOAA-7. *Int. Journ. Remote Sens.*, **6**, 1435–1444.
- Pruppacher, H. R., 1980: Microstructure of atmospheric clouds and precipitation. *Clouds: Their Formation, Optical Properties, and Effects*, P. Hobbs and A. Deepak, Eds. 93–185.
- Rast, M., 1989: Status of the first European Polar Platform Mission. *The Earth Observer*, **1**, 7 pp.
- Rothman, L. S., R. R. Gamache, A. Barbe, A. Goldman, J. R. Gillis, L. R. Brown, R. A. Toth, J.-M. Flaud and C. Camy-Peyret, 1983: AFGl atmospheric absorption line parameters compilation: 1982 edition. *Appl. Opt.*, **22**, 2247–2256.
- Saiedy, F., H. Jacobowitz and D. Q. Wark, 1967: On cloud-top determination from Gemini-5. *J. Atmos. Sci.*, **24**, 63–69.
- Shenk, W. E., R. J. Holub and R. A. Neff, 1975: Stereographic cloud analysis from Apollo-6 photographs over a cold front. *Bull. Amer. Meteor. Soc.*, **56**, 4–16.
- Smith, W. L., H. W. Woreff and C. M. Haysen, 1973: Meteorological extractions from the Nimbus-5 ITPR experiment. *Proc. CNES Conference, Paris*, 207–217.
- Stephens, G. L., 1979: Optical properties of eight water cloud types, Tech Paper, No. 36 [Available from Commonwealth Scientific and Industrial Research Organisation, Division of Atmospheric Physics, Australia.]
- Vonder Haar, T. H., and D. W. Reynolds, 1974: A bispectral method for inferring cloud amount and cloud top temperature using satellite data. *Sixth Conf. on Aerospace and Aeronautical Meteorology*, Amer. Meteor. Soc., 190 pp.
- Wark, D. Q., and D. M. Mercer, 1965: Absorption in the atmosphere by the oxygen A-band. *Appl. Opt.*, **4**, 839 pp.
- WCP-55, 1983: Reprt of the experts meeting on aerosols and their climate effects, Williamsburg, VA, A. Deepak and H. E. Gerber, Eds., WMO-CAS and Radiation Commission of IAMAP.
- Wu, M. L., 1985: Remote sensing of cloud-top pressure using reflected solar radiation in the oxygen A-band. *J. Appl. Meteor.*, **24**, 539–546.
- Yamaoto, G., and D. Q. Wark, 1961: Discussion of the letter by R. A. Hanel: Determination of cloud altitude from a satellite. *J. Geophys. Res.*, **66**, 3596 pp.